Calculation for Stator Loss of High-Speed Permanent Magnet Synchronous Machine in Torque-speed Envelope and Restraint Approach for Circulating Current in Windings

Yanan Yu, Deliang Liang, *Senior Member,* Zhe Liang, and Qiji Ze

***Abstract*—Iron loss and copper loss are the significant parts of electrical loss of machines, which are the major parts particularly under high frequency condition. High-speed permanent magnet synchronous machines (HS-PMSM) have the benefits of high power density, high efficiency and wide speed range. Which causes the calculation for iron loss and copper loss in whole operating range complex. By analyzing the components and influencing factors of iron loss and copper loss in stator, we have deduced the calculation formula of iron loss and copper loss in whole operating range based on the analytical solution and finite element approach (EFA) solution. According to the calculation solution, taking the influence of operating temperature on the iron loss and copper loss into account, we propose a temperature correction factor and establish the calculation method for the iron loss and copper loss with temperature influences. Finally, by the conductor transposition, we restrain the circulating current under high-frequency operating condition.**

***Index Terms*—Circulating, high-speed permanent magnet machines, iron loss, torque-speed envelope.**

I. Introduction

MACHINES are widely used in many applications such as industry, national defense, transportation, agriculture, municipal administration and so on. As the most power-consuming devices, they are tending to high speed, high efficiency, high power density, intelligence and integration. The volume of high-speed machines are smaller than low-speed machines with the same output power due to their high power density, which can effectively save materials when manufacturing machines. A high-speed machine can be directly connected with a prime mover or a load device without the conventional mechanical transmission devices, which can reduce the vibration and noise to improve the efficiency of the drive system. Another advantage of high-speed machines is fast speed dynamic response due to their small moment of inertia. The types of. high-speed machines include induction machines, permanent-magnet machines and switched reluctance machines [1]-[3]. Among these machines, high-speed permanent-magnet machines without exciting field windings are favored because of the advantages of high density, high efficiency and wide speed range. Large-capacity, high-speed motor/generators are currently the research hotspots for advanced power equipment manufacturing in the world. In the field of defense, military, and new energy power equipment, the replacement of traditional mid- and low-speed motor/generators with high-speed permanent magnet motors/generators is an inevitable trend for the development of high-end power equipment in the future, and has become a leader to leading a new generation of high-end power equipment technology [4]-[5].

The analytical methods and numerical methods commonly used at present can well calculate the core loss under a certain working condition [6]-[8], but due to the wide speed range of the high-speed permanent magnet machines, the operating frequency range is relatively wide, the use of a certain frequency equivalent to other frequencies will cause larger errors, and it takes a lot of time to calculate the losses at all frequencies one by one. Another existing calculation method does not properly take the influence of temperature factors into account. Changes in the operating temperature will affect the core resistivity, thus affecting the eddy current loss. The operating temperature will also cause changes in the remanence of the permanent magnet, resulting in changes in the core flux density and no-load back-EMF, which will affect core losses

II. Calculation for Stator Loss in Torque-speed Envelope

The main formulas for stator core loss of permanent magnet motor include Stermanz formula and Bottorti formula. These formulae calculate the core loss of a working point of the permanent magnet synchronous motor [9]. It is impossible to quickly calculate the loss distribution in the whole work area,

Manuscript was submitted for review on 07, May, 2018.

This work was supported by the National Natural Science Foundation of China (51677144).

All authors are with the State Key Laboratory of Electrical Insulation and Power Equipment, School of Electrical Engineering, Xi'an Jiaotong University, Xi'an 710049, China (e-mail: dlliang@mail.xjtu.edu.cn).

Digital Object Identifier 10.30941/CESTEMS.2018.00026

and it is impossible to calculate the influence of the temperature change on the loss. With the continuous improvement of the computing speed of computers and the progress of related software, the use of finite element method to calculate the core loss of the motor has become the preferred method. However, the above problems also exist.

Through the analysis of the magnetic field lines of the permanent magnet motor, it can be seen that the distribution of the magnetic field lines is divided into two steps. The first is the main magnetic flux, that is, the teeth and the yoke that pass through the stator, and it forms a magnetic chain with the stator winding coils. The second is that only the teeth of the stator flow through the stator and are not interlinked with the stator coils, as shown in the figure 1. It can be considered that the loss produced by the stator core of the motor is a superposition of the core losses generated by the two operating modes with different magnetic circuits.

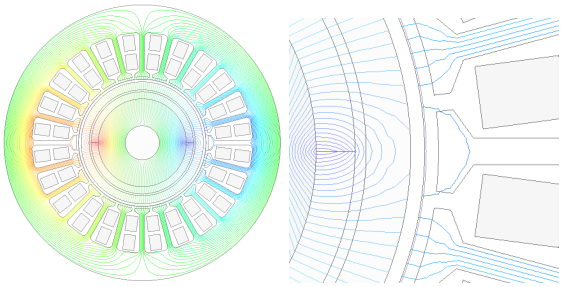

Fig.1. magnetic field distributions.

The stator core loss caused by the first main magnetic flux is directly related to its magnetic flux amplitude and the resulting stator winding induced electromotive force. Similar to the stator core loss of a conventional induction motor, it can be represented by a polynomial approximation of the induced voltage E0. Voltage E0 is the voltage after the winding voltage drop. The magnetic circuit in the second case will cause additional core losses at the top of the teeth of the stator core, depending on the strength of the magnetic field applied to the stator and the corresponding equivalent voltage E0. And E0 and Ed can be determined by the motor d-q axis phasor diagram.

According to the improved Steinmet formula [10], the hysteresis loss, eddy current loss, and stray loss which are the components of the stator core loss can be expressed as

$$W_{Fe} = k_h B_m^2 f k_f + \sum_{\Delta T}\left[\sigma\frac{d^2}{12}\left(\frac{\Delta B}{\Delta T}\right)^2 + k_e\left(\frac{\Delta B}{\Delta T}\right)^{1.5}\right]\Delta T f k_f \tag{1}$$

where, k_h is hysteresis loss factor, B_m is maximum value of magnetic field strength in one electrical period, ΔB is increment of magnetic field intensity with one step, k_f is lamination coefficient, σ is conductivity of silicon steel sheet,D is length of stator core iron, k_e is stray loss, ΔT is time step.

Using the finite element method, the hysteresis loss, eddy current loss, stray loss, ideal open-circuit back EMF and ideal short-circuit current can be respectively calculated under ideal open circuit and ideal short circuit conditions, ignoring the influence of the resistance of the stator winding and the end leakage inductance. The two losses of the stator core combined with the Steinmet equation can be expressed as follows:

$$P_{iron1} = \frac{a_h f}{E_{prms}} E_0 + \frac{a_j f^2}{E_{prms}^{\ 2}} E_0^{\ 2} + \frac{a_{ex} f^{1.5}}{E_{prms}^{\ 1.5}} E_0^{\ 1.5} \tag{2}$$

$$P_{iron2} = \frac{b_h f}{E_{prms}} E_d + \frac{b_j f^2}{E_{prms}^{\ 2}} E_d^{\ 2} + \frac{b_{ex} f^{1.5}}{E_{prms}^{\ 1.5}} E_d^{\ 1.5} \tag{3}$$

where, f is frequency, E_{prms} is Back-EMF coefficient is line voltage can be expressed in V/rpm unit.

Polynomial coefficients can be obtained for hysteresis loss, eddy current loss, and stray loss for an ideal open circuit and an ideal short circuit at any frequency.

Through the finite element analysis, E_{prms} can be calculated under the ideal open circuit situation. The voltage of the stable working point where the above formula is located can be obtained through the phasor diagram of the motor's direct-axis phasor. Considering that most high-speed permanent-magnet motors use the surface-mount structure, the stator armature reaction can be decided by the corresponding ideal short-circuit current. Current can be simulated by finite element analysis.

$$I_q = \frac{T}{K_T} \tag{4}$$

$$E_0 = E_{prms}\sqrt{\left(1-\frac{I_q}{I_{SC}}\right)^2 + \left(\frac{I_q}{I_{SC}}\right)^2} \tag{5}$$

$$E_0 = E_{prms}\sqrt{\left(1-\frac{K_T}{I_{SC}T}\right)^2 + \left(\frac{K_T}{I_{SC}T}\right)^2} \tag{6}$$

$$E_d = E_{prms}\frac{I_q}{I_{SC}} \tag{7}$$

$$E_d = E_{prms}\frac{K_T}{T} \tag{8}$$

Where, T is torque, I_q is d-axis current, K_T is torque constant, I_{SC} is ideal short-circuit current.

The two parts of the stator core loss distribution can be expressed as:

$$\begin{aligned} P_{iron1} = {} & a_h f\sqrt{\left(1-\frac{T}{K_T I_{SC}}\right)^2 + \left(\frac{T}{K_T I_{SC}}\right)^2} \\ & + a_j f^2\left(\left(1-\frac{T}{K_T I_{SC}}\right)^2 + \left(\frac{T}{K_T I_{SC}}\right)^2\right) \\ & + a_{ex} f^{1.5}\left(\sqrt{\left(1-\frac{T}{K_T I_{SC}}\right)^2 + \left(\frac{T}{K_T I_{SC}}\right)^2}\right)^{1.5} \end{aligned} \tag{9}$$

$$\begin{aligned} P_{iron2} = {} & b_h f\frac{T}{K_T I_{SC}} + b_j f^2\left(\frac{T}{K_T I_{SC}}\right)^2 \\ & + b_{ex} f^{1.5}\left(\frac{T}{K_T I_{SC}}\right)^{1.5} \end{aligned} \tag{10}$$

For permanent magnet motors，

$$\psi = \frac{E_{\phi 0}}{\omega_e} \tag{11}$$

$$E_{\phi 0} = \frac{\sqrt{2} E_{prms} n}{\sqrt{3}} \tag{12}$$

$$\omega_e = 2\pi \mathrm{p} n / 60 \tag{13}$$

$$\psi = 7.797 \frac{E_{prms}}{p} \tag{14}$$

$$T_e = \frac{3}{2} p \psi i_q \tag{15}$$

$$K_T = \frac{T_e}{i_q} = \frac{3}{2} p \psi \tag{16}$$

Where，ψ is flux caused by permanent magnet，P is pole pairs.

The motor torque constant and no-load back-EMF coefficient have the following relationship:

$$K_T = 11.696 E_{prms} \tag{17}$$

The motor stator losses can be written as

$$P_{iron1} = a_h f \left(\left(1 - \frac{T}{11.696 E_{prms} I_{SC}} \right)^2 + \left(\frac{T}{11.696 E_{prms} I_{SC}} \right)^2 \right)^{\frac{1}{2}} + a_j f^2 \left(\left(1 - \frac{T}{11.696 E_{prms} I_{SC}} \right)^2 + \left(\frac{T}{11.696 E_{prms} I_{SC}} \right)^2 \right) + a_{ex} f^{1.5} \left(\left(1 - \frac{T}{11.696 E_{prms} I_{SC}} \right)^2 + \left(\frac{T}{11.696 E_{prms} I_{SC}} \right)^2 \right)^{\frac{3}{2}} \tag{18}$$

$$P_{iron2} = b_h f \frac{T}{11.696 E_{prms} I_{SC}} + b_j f^2 \left(\frac{T}{11.696 E_{prms} I_{SC}} \right)^2 + b_{ex} f^{1.5} \left(\frac{T}{11.696 E_{prms} I_{SC}} \right)^{1.5} \tag{19}$$

Through the finite element simulation results at a certain frequency, the coefficient of formula 18 and formula 19 can be obtained, and the stator core loss at any frequency and arbitrary torque can be obtained. Without the loss of one simulation at different frequencies, the workload is reduced and the calculation efficiency is improved.

III. Influence of the Operating Temperature on the Loss of Stator Core

The influence of stator iron core temperature on the core eddy current loss is due to temperature-induced changes in core material resistivity, so the temperature-induced eddy current loss changes can be attributed to temperature-induced resistivity changes, eddy current loss changes and resistivity changes inversely [11]-[12], it is available

$$\frac{P_{e|T}}{P_{e|T_0}} = \frac{\rho_{0-Fe}}{\rho_{0-Fe}(\alpha(T - T_0) + 1)} \tag{20}$$

$$\rho_{Fe} = \rho_{0-Fe}(\alpha(T - T_0) + 1) \tag{21}$$

$$P_{e|T} = \frac{P_{e|T_0}}{\alpha(T - T_0) + 1} \tag{22}$$

Where, $P_{e|T}$ is iron core eddy current loss when the temperature is T, $P_{e|T_0}$ is iron core eddy current loss when the temperature is T0, ρ_{0-Fe} is the resistivity of the iron core material when the temperature is T0, α is the temperature coefficient of the resistivity of the iron core material.

The hysteresis loss is caused by the material's B-H curve. A hysteresis loss occurs for every B-H curve of the core material. Because the effect of temperature on the hysteresis loss of the stator core must be analyzed, the effect of temperature on B-H characteristic curve must be analyzed.

The loss caused by one B-H cycle per unit volume of core material is

$$P_H = \oint H dB \tag{23}$$

$$B = \mu H \tag{24}$$

$$P_H = \mu \oint H^2 dH \tag{25}$$

Therefore, by researching the influence of temperature on the relative permeability of iron core material, the influence of temperature on the characteristic B-H curve of iron core material can be obtained. Studies in the literature [13]-[14] have shown that the amplitude of μ with temperature changes in the range of 0-500°C is very small, but when the temperature is higher than 500°C, it decreases sharply with increasing temperature. This temperature range includes the normal operating temperature range of the permanent magnet motor. When the motor temperature rises to the inflection point of μ, the permanent magnet of the permanent magnet motor has already been irreversibly demagnetized due to an excessively high temperature, and the insulation of the motor has been damage also due to an excessively high temperature. For common permanent magnet motors, relative permeability μ_r does not change with temperature as the motor temperature rises.

It can be seen from the above formula 18 and formula 19 that the hysteresis loss of the stator core is not only related to the relative magnetic permeability μ, but also to the strength of the magnetic field. In the case where the motor structure is

determined, the magnetic field strength is related to the remanence of the permanent magnet B_r, and the permanent magnet follows. As the temperature rises, the magnetic properties gradually decrease.

Permanent magnets such as neodymium iron boron, the change of the remanence of the permanent magnet directly affects the back EMF generated by the windings, and they have a linear relationship. Because the temperature and the winding back EMF also have a linear relationship, so it is possible to calculate the stator core loss caused by the change of permanent magnet performance caused by temperature changes.

There are no-load back-EMF E_{prms} in the formula 18 and formula 19, and its relationship with temperature change is as follows:

$$E_{prms}\left|T_{PM}=\left(\delta\left(T_{PM}-T_{PM0}\right)+1\right)E_{prms}\right|T_{PM0} \quad (26)$$

Where, $E_{prms}\left|T_{PM0}\right.$ is no-load back EMF when the operating temperature is T_{PM0}, $E_{prms}\left|T_{PM}\right.$ is back EMF when the operating temperature is T_{PM}, δ is the temperature coefficient of remanence of permanet-magnet.

Then the influence of operature temperature on the stator iron loss can be obtain by bring $E_{prms}\left|T_{PM}\right.$ into $E_{prms}\left|T_{PM0}\right.$

$$\begin{aligned}P_{iron1}=&a_h f\sqrt{\left(1-\frac{T}{11.696\left(\delta\left(T_{PM}-T_{PM0}\right)+1\right)E_{prms}I_{SC}}\right)^2+\left(\frac{T}{11.696\left(\delta\left(T_{PM}-T_{PM0}\right)+1\right)E_{prms}I_{SC}}\right)^2}\\&+\frac{a_j f^2}{\alpha(T-T_0)+1}\left(\left(1-\frac{T}{11.696\left(\delta\left(T_{PM}-T_{PM0}\right)+1\right)E_{prms}I_{SC}}\right)^2+\left(\frac{T}{11.696\left(\delta\left(T_{PM}-T_{PM0}\right)+1\right)E_{prms}I_{SC}}\right)^2\right)\\&+a_{ex}f^{1.5}\left(\sqrt{\left(1-\frac{T}{11.696\left(\delta\left(T_{PM}-T_{PM0}\right)+1\right)E_{prms}I_{SC}}\right)^2+\left(\frac{T}{11.696\left(\delta\left(T_{PM}-T_{PM0}\right)+1\right)E_{prms}I_{SC}}\right)^2}\right)^{1.5}\end{aligned} \quad (27)$$

$$\begin{aligned}P_{iron2}=&b_h f\frac{T}{11.696\left(\delta\left(T_{PM}-T_{PM0}\right)+1\right)E_{prms}I_{SC}}+\frac{b_j f^2\left(\dfrac{T}{11.696\left(\delta\left(T_{PM}-T_{PM0}\right)+1\right)E_{prms}I_{SC}}\right)^2}{\alpha(T-T_0)+1}\\&+b_{ex}f^{1.5}\left(\frac{T}{11.696\left(\delta\left(T_{PM}-T_{PM0}\right)+1\right)E_{prms}I_{SC}}\right)^{1.5}\end{aligned} \quad (28)$$

Assuming that the stray loss of the motor does not change with the change of the operating temperature of the motor, the formula for calculating the global core loss when considering the change of the operating temperature of the motor can be obtained:

$$\begin{aligned}P_{iron1}=&a_h f\sqrt{\left(1-\frac{T}{11.696\left(\delta\left(T_{PM}-T_{PM0}\right)+1\right)E_{prms}I_{SC}}\right)^2+\left(\frac{T}{11.696\left(\delta\left(T_{PM}-T_{PM0}\right)+1\right)E_{prms}I_{SC}}\right)^2}\\&+a_j f^2\left(\left(1-\frac{T}{11.696\left(\delta\left(T_{PM}-T_{PM0}\right)+1\right)E_{prms}I_{SC}}\right)^2+\left(\frac{T}{11.696\left(\delta\left(T_{PM}-T_{PM0}\right)+1\right)E_{prms}I_{SC}}\right)^2\right)\\&+a_{ex}f^{1.5}\left(\sqrt{\left(1-\frac{T}{11.696\left(\delta\left(T_{PM}-T_{PM0}\right)+1\right)E_{prms}I_{SC}}\right)^2+\left(\frac{T}{11.696\left(\delta\left(T_{PM}-T_{PM0}\right)+1\right)E_{prms}I_{SC}}\right)^2}\right)^{1.5}\end{aligned} \quad (29)$$

$$\begin{aligned}P_{iron2}=&b_h f\frac{T}{11.696\left(\delta\left(T_{PM}-T_{PM0}\right)+1\right)E_{prms}I_{SC}}+b_j f^2\left(\frac{T}{11.696\left(\delta\left(T_{PM}-T_{PM0}\right)+1\right)E_{prms}I_{SC}}\right)^2\\&+b_{ex}f^{1.5}\left(\frac{T}{11.696\left(\delta\left(T_{PM}-T_{PM0}\right)+1\right)E_{prms}I_{SC}}\right)^{1.5}\end{aligned} \quad (30)$$

IV. HIGH SPEED PERMANENT MAGNET SYNCHRONOUS MOTOR STATOR WINDING LOSS

When AC currents flow through a conductor, a time-varying magnetic field is generated in a plane perpendicular to the current. This time-varying magnetic field induces eddy currents in the conductor and other conductors parallel to the conductor if the size of the conductor is smaller than When the frequency of the large time-varying current is high, the eddy current induced by the time-varying magnetic field in the conductor will hinder the penetration of the magnetic field in the conductor, and only allow the magnetic field to penetrate into a certain depth of the conductor, so that the added time-varying current Induced eddy currents are superimposed on the surface of the conductor. Currents tend to be on the surface of the conductor, and no current passes through the center of the

conductor [15]-[18]. This is the skin effect caused by the high-frequency current. If the winding is composed of several wires, the time-varying magnetic field produced by each wire will affect the immediately adjacent wire while the high-frequency current causes the skin effect. As a result, the current on the adjacent wire does not uniformly flow through the wire cross-section, but is biased. On one side, this is the proximity effect, as shown in the Fig. 2.

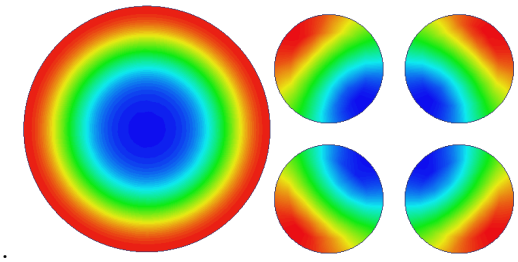

(a) The skin effect (b) The proximity effect

Fig. 2. The skin effect and The proximity effect.

When the AC current passes through the conductor, an eddy current will be generated in the conductor itself [19]-[20]. This eddy current is caused by the alternating magnetic field generated by the alternating current itself in the conductor, thus affecting the even distribution of the conductor at the cross section. .

$$\delta = \frac{1}{\sqrt{\pi f \mu \sigma}} \tag{31}$$

With skin depth, we can think that most of the current is concentrated in the conductors in this thickness range.

For AC motors, because the number of leakage fluxes along the high cross section of the wire is not equal, the resulting induced potential is not the same, creating a vortex within the wire. The current is unevenly distributed across the cross-section of the wire, and the current in the wire tends to the surface, creating a skin effect, making the AC resistance larger than the DC resistance [21].

To facilitate analysis of the skin effect of windings in AC motor slots by analytical methods, make the following assumptions:

1. Assume that current is sinusoidally changing with time;
2. The magnetic field strength vector in the tank is parallel to the bottom of the tank;
3. ignore the magnetic pressure drop of the stator core, ignore the insulating layer of the conductor.

Stator stator slots and windings are shown Fig. 3.

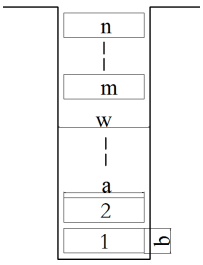

Fig 3. Slot distribution diagram.

we define: $\eta = a / w$,as the transverse groove ratio of conductor, and equivalent skin depth of the conductor is

$$\delta' = \frac{1}{\sqrt{\eta \pi f \mu \sigma}} \tag{32}$$

According to Ampere's Law of Circuits and Faraday's Law of Induction, when the sinusoidal current is passed through the stator windings, the relation between the magnetic field strength H_x and the current density J_z in the conductor can be obtained.

$$\frac{\partial^2 H_x}{\partial y^2} = k^2 H_x \tag{33}$$

$$\frac{\partial H_x}{\partial y} = -\eta J_z \tag{34}$$

$$k = \frac{1+j}{\delta'} \tag{35}$$

Where: δ' is penetration depth, μ is relative permeability, σ is the conductivity of Winding material,

The relationship between electric field strength Ez and current density Jz is:

$$E_z = \frac{J_z}{\sigma} \tag{36}$$

The active power of the mth wire is:

$$\begin{aligned} P = &\frac{1}{2} abl \cdot \mathrm{Re}\left(E_z H_z\right)_{y=(m-1)b} \\ &-\frac{1}{2} abl \cdot \mathrm{Re}\left(E_z H_z\right)_{y=mb} \end{aligned} \tag{37}$$

The AC resistance and DC resistance of the mth wire are:

$$R_{AC} = \frac{2P}{I_m} \tag{38}$$

$$R_{DC} = \frac{l}{\sigma ab} \tag{39}$$

Where, I_m is the amplitude of AC current,L is calculated length of winding wire,From the above formula, the mth wire resistance increase coefficient can be obtained:

$$\begin{aligned} K_{pm} = \frac{R_{AC}}{R_{DC}} = &\left(\frac{b}{\delta'}\right) \frac{sh2\left(\frac{b}{\delta'}\right) + \sin 2\left(\frac{b}{\delta'}\right)}{ch2\left(\frac{b}{\delta'}\right) - \cos 2\left(\frac{b}{\delta'}\right)} \\ &+ m(m-1) 2\left(\frac{b}{\delta'}\right) \frac{sh2\left(\frac{b}{\delta'}\right) - \sin 2\left(\frac{b}{\delta'}\right)}{ch2\left(\frac{b}{\delta'}\right) + \cos 2\left(\frac{b}{\delta'}\right)} \end{aligned} \tag{40}$$

The average increase coefficient of n wire resistance in the slot is

$$K_p = \frac{1}{n} \sum_{1}^{n} K_{pm} \tag{41}$$

It can be seen from the above equation that the skin effect of the stator winding wire of the AC motor increases as the conductivity and frequency increase, and the skin effect of the wire along the slot bottom to the slot top direction gradually increases, and the skin effect of the wire is most obvious in the conductors at the slot top of the stator,as shown in Fig 4.

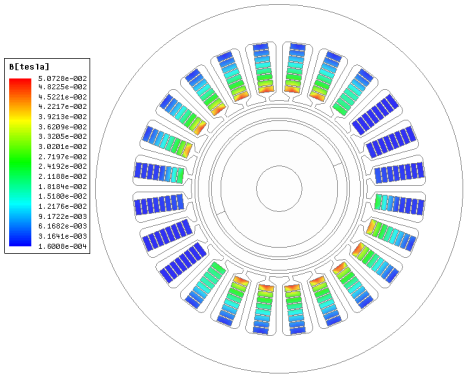

Fig 4. The skin effect and The proximity effect.

V. INFLUENCE OF TEMPERATURE ON HIGH-FREQUENCY ADDITIONAL LOSS

Through the analysis in the previous section, under the high-frequency alternating current, the loss of the stator winding wire can be divided into AC loss and DC loss [22]-[23]. Then the winding loss formula can be written as

$$P = I^2 R_{DC}\left(\frac{R_{AC}}{R_{DC}} - 1\right) + I^2 R_{DC} \tag{42}$$

$$\frac{R_{AC}}{R_{DC}} = K_p \tag{43}$$

The relationship between the temperature and the resistivity of the copper conductor is as follows:

$$\rho_{CuT} = \rho_{Cu0}\left(\alpha\left(T - T_0\right) + 1\right) \tag{44}$$

Where,: ρ_{Cu0} is the resistivity of the copper when the temperature is T_0, ρ_{CuT} is the resistivity of the copper when the temperature is T, α is the temperature coefficient of resistivity of the copper conductor

According to the relationship between stator winding loss and stator current of the AC motor in the reference [24], the temperature coefficient can be substituted into the winding loss formula, and the winding loss calculation formula when the working temperature of the permanent magnet synchronous motor is T can be obtained.

$$\begin{aligned} P_T = &\frac{I^2 R_{DC}|_{T_0}}{\sqrt{\alpha\left(T - T_0\right) + 1}}\left(K_p|_{T_0} - 1\right) \\ &+ I^2 R_{DC}|_{T_0}\left(\alpha\left(T - T_0\right) + 1\right) \end{aligned} \tag{45}$$

where: $R_{DC}|_{T_0}$ is the DC resistance of the stator winding when the reference temperature is T_0; $K_p|_{T_0}$ is the ratio of the AC equivalent resistance to the DC resistance when the reference temperature is T_0.

From the above equation, the ratio of AC winding losses to DC winding losses when the motor operating temperature is T is:

$$\frac{P_{AC}}{P_{DC}}|_T = K_p|_T = \frac{\left(K_p|_{T_0} - 1\right)}{\left(1 + \alpha\left(T - T_0\right)\right)^{\frac{3}{2}}} + 1 \tag{46}$$

When the working temperature of permanent magnet synchronous AC motor is T, the loss of DC winding is as follows:

$$\frac{P_{DC}|_T}{P_{DC}|_{T_0}} = 1 + \alpha\left(T - T_0\right) \tag{47}$$

Therefore, when the operating temperature of the permanent magnet synchronous motor is T, the loss of the AC winding and the loss of the DC winding when the operating temperature of the permanent magnet synchronous motor is T_0 as follows:

$$\frac{P_{AC}|_T}{P_{DC}|_{T_0}} = \frac{\left(K_p|_{T_0} - 1\right)}{\sqrt{1 + \alpha\left(T - T_0\right)}} + 1 + \alpha\left(T - T_0\right) \tag{48}$$

Finally, when the permanent magnet synchronous motor operating temperature is T, the stator winding loss is

$$\begin{aligned} P_T = &P_{DC}|_{T_0}\frac{\left(K_p|_{T_0} - 1\right)}{\sqrt{\alpha\left(T - T_0\right) + 1}} \\ &+ P_{DC}|_{T_0}\left(\alpha\left(T - T_0\right) + 1\right) \end{aligned} \tag{49}$$

Through finite element calculations or experimental measurements, AC winding losses and DC winding losses at a certain current and temperature at a certain frequency are obtained to ensure that the effective value and the DC current value of the AC current are equal, and the loss value can be obtained. With the ratio of the AC/DC resistance, $K_p|_{T_0}$, at this temperature T_0, the winding losses of the PMSM at different frequencies and temperatures can be obtained by the above formula.

VI. RESTRAINT APPROACH FOR CIRCULATING CURRENT IN WINDINGS

In the high-speed permanent magnet motor, because the speed is high, the number of series turns per phase is often very small, and it is more suitable to use multiple parallel branch windings. However, according to the above analysis, the wires near the stator slots are affected by the skin effect and proximity effects have a greater impact. Compared to the conductors at the bottom of the trench, the current in the upper part of the trench tends to concentrate on the surface, which can cause unbalanced circulation and eventually lead to inconsistent currents in the parallel conductors [25]-[26]. In the high-speed permanent magnet motor, in order to reduce the eddy current loss of the winding conductor, thin wires are generally adopted. Each turn of the conductor is usually composed of several parallel strands. Each parallel strand of the coil is stacked in the height direction of the stator slot. In the stator slots, the magnetic field weakens in the height direction of the stator slot, that is, in the radial direction. The difference in magnetic density between the top and bottom of the slot is relatively large, generally up to 0.25T. Considering the difference bewteen the positions of the conductors in the slots and the winding skin effect and proximity effect under high frequency, will have a great circulating current, which increases the loss of windings[27].

A high-speed permanent magnet motor model with 8 internal

conductors per slot has been built. To simplify the calculation, single-layer windings are modeled and only the A-phase windings are retained for simulation, as shown in the figure. The schematic diagram of the arrangement of the A-phase winding in the slots is shown in the figure. The 8 conductors are wound in one turn. The 8 conductors of each coil are located in different positions of the magnetic field in the stator slots [28]. The induced EMF of conductors have a large difference, and the permanent magnet high-speed motor is operated under high-frequency operation condition. The skin effect and proximity effect affected by the conductors will increase the difference in induced EMF between the wires. Since these 8 conductors eventually form a coil in parallel, a large circulating current will flow though these conductors [29].

Simulation of the model at 24,000 rpm gives the values of the induced electromotive force generated by the 8 conductors in a rotating magnetic field, as shown in the figure. From the Fig. 5, it can be seen that there is a difference between the values of the induced EMF generated by the 8 conductors, and the maximum value can be more than 9V. The conductor with the largest induced EMF is the nearest to the slot top.

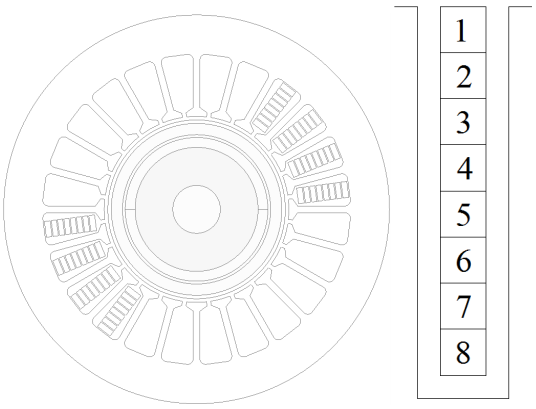

Fig 5. 24000rpm HPMSM Model.

The EMF generated by the conductor 1, due to the fact that the density of the magnetic field at the location of the conductor 1 is the largest and the conductor is located at the top, and the influence of the skin effect and the proximity effect is relatively small. The conductor with the smallest induced EMF is not the conductor 8 but the conductor 7 at the bottom of the slot. This is because of the skin effect and proximity effect of the conductor under high frequency conditions, except that the density of the magnetic field at the conductor affects the induced electromotive force of the conductor. It also affects the induced electromotive force of the conductor. The conductor 8 is at the bottom of the winding. The skin effect and the proximity effect are relatively small. Compared to the conductor 7, the influence of the conductor 7 is relatively large, so the induced electromotive force of the conductor is also relatively small. The difference between the induced electromotive force of conductor 1 and conductor 7 is as shown in the figure. The maximum amplitude is 10.46484V,as shown Fig6-7, because the resistance value of the winding is relatively small. This potential difference can generate tens of amps of internal winding circulation and increase the loss of the winding.

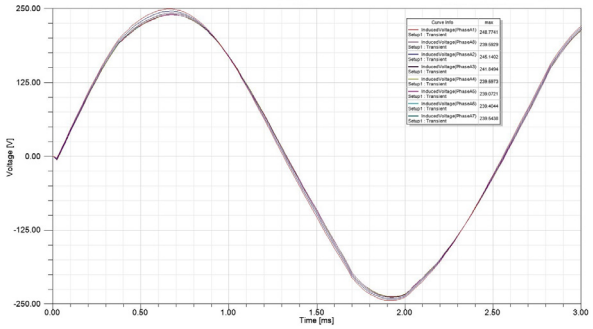

Fig. 6. Induced voltage of the eight conductor.

The EMF generated by the conductor 1, due to the fact that the density of the magnetic field at the location of the conductor 1 is the largest and the conductor is located at the top, and the influence of the skin effect and the proximity effect is relatively small. The conductor with the smallest induced EMF is not the conductor 8 but the conductor 7 at the bottom of the slot. This is because of the skin effect and proximity effect of the conductor under high frequency conditions, except that the density of the magnetic field at the conductor affects the induced electromotive force of the conductor. It also affects the induced electromotive force of the conductor. The conductor 8 is at the bottom of the winding. The skin effect and the proximity effect are relatively small. Compared to the conductor 7, the influence of the conductor 7 is relatively large, so the induced electromotive force of the conductor is also relatively small. The difference between the induced electromotive force of conductor 1 and conductor 7 is as shown in the figure. The maximum amplitude is 10.46484V, because the resistance value of the winding is relatively small. This potential difference can generate tens of amps of internal winding circulation and increase the loss of the winding.

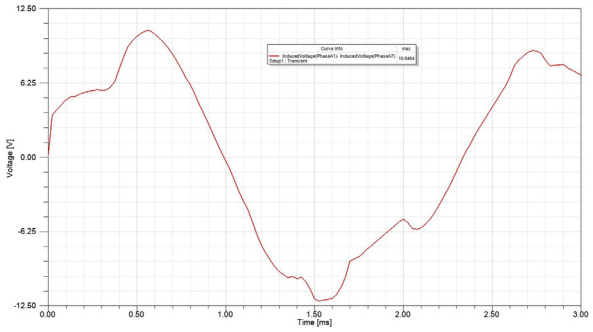

Fig 7. Maximum Induced Voltage between eight conductor.

In the production, the slot conductors can be coiled with transposing coils. This is mainly used to restrain the skin effect caused by high-frequency currents, and the wires are transposed through the slots. The circulating current has been weakened, the loss is reduced, or the windings are star-connected, and a separate neutral point is set for each parallel branch. The neutral points of different parallel branches are insulated from each other and are not connected to each other. the circulating current caused by the unbalanced branch can be effectively restrained.

Multiplexing of the parallel branch to set the neutral point alone will result in complex end processes. The simplest and

most effective method to eliminate the circulation is to perform transposition of the conductor in the slot. The schematic diagram of the transposition of the conductor in the slot is shown in the Fig. 8. Each turn consists of 8 conductors. The 8 conductors in the radial direction are transposed between the layers, so that the conductor distribution of each winding coil is in different positions in the magnetic field, so as to ensure There is basically no difference in the induced electromotive force of each conductor after transposition.

1	1	1	1
2	2	2	2
3	3	3	3
4	4	4	4
5	5	5	5
6	6	6	6
7	7	7	7
8	8	8	8

(a) transposing coils before

1	5	8	4
2	6	7	3
5	1	4	8
6	2	3	7
7	3	2	6
8	4	1	5
3	7	6	2
4	8	5	1

(b) transposing coils after

Fig 8. conductor transposition of each coil at two pair-pole.

As shown in the figure, the induced electromotive force of a pair of lower pole conductors after transposition in the slot can be clearly seen that the difference of the induced potentials of the eight conductors is eliminated, and the difference between the maximum and the minimum value of the induced potential is shown in the Fig9-10. The maximum amplitude of the induced potential is less than 30mV. It can be considered that the induced potential difference is basically eliminated and the circulation can be effectively suppressed.

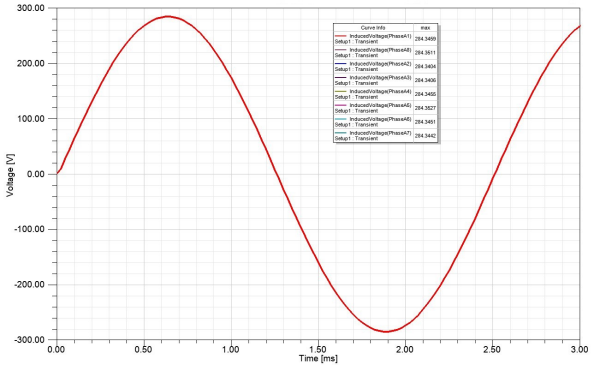

Fig 9. Induced voltage of the eight conductor.

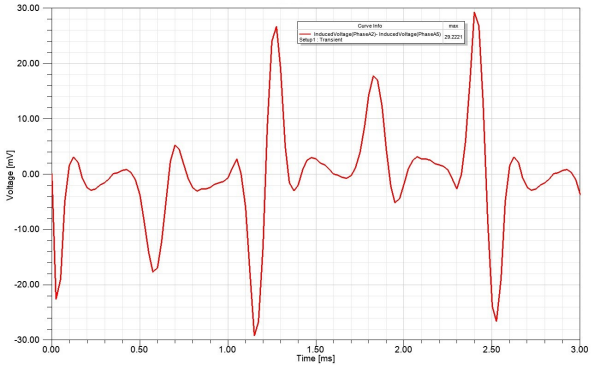

Fig 10. Maximum Induced Voltage between eight conductor.

VII. CONCLUSION

High-speed permanent magnet synchronous motor has characteristics of high speed, wide speed range, and large frequency range. This paper analyzes the composition and influencing factors of stator core loss and winding loss, and deduces stator loss in the torque speed envelope by analytical method combined with finite element method. The calculation method of the winding loss and the influence of the operating temperature on the calculation of the core loss and the winding loss were analyzed. The temperature correction coefficient was proposed and calculation method for computing the temperature factor in the torque-speed envelope was obtained. Finally, it is proposed that proper winding coil wire transposition technique used to reduce the internal circulating current caused by the induced voltage difference of the wire in different positions in the slots caused by high frequency, reduce the additional copper consumption and improve the reliability of the high-speed permanent magnet synchronous motor.

REFERENCES

[1] C Zwyssig, J. W. Kolar, W, Thaler, M. Vohrer, “Designofa100W,500000rpm permanent-magnet generator for Mesoscale Gas Turbines, in *Proceedings of IEEE IAS Annual Meeting* 2005, pp. 253-260.

[2] Thomas Baumgartner, and Johann W. Kolar, “Multivariable State Feedback Control of a 500 000r/min Self-Bearing Permanent-Magnet Motor”, *IEEE/ASME Transactions on Mechatronics*, vol. 20, no. 3, pp.1149-1159, June, 2015.

[3] Sunil Kumar, Wenliang Zhao, Zhentao S. Du, Thomas A Lipo, and Byung-Il Kwon, “Design of Ultrahigh Speed Axial-Flux Permanent Magnet Machine With Sinusoidal Back EMF for Energy Storage Application”, *IEEE Transactions on Magnetics*, vol. 51, no. 11, November 2015, Article #: 8113904.

[4] O. Aglen, “Back-to-Back tests of a high-speed generator”, in *Proceeding of the IEEE International Electric Machines and Drives Conferences 2003*, pp. 1084-1090, 2003.

[5] Gerada D, Mebarki A, Mokhadkar R P, Brown N L, Gerada C. “Design issues of high-speed permanent magnet machines for high-temperature applications”. in *Electric Machines and Drives Conference2009*, pp. 1036-1042, 2009:

[6] Munteanu G, Binder A, Schneider T. “Loss measurement of a 40kW high-speed bearing less PM synchronous motor”. in *IEEE Energy Conversion Congress and Exposition*, pp: 22-929, 2011.

[7] Fengge Zhang, Guanghui Du, TianyuWang, Guangwei Liu, and Wenping Cao. “Rotor Retaining Sleeve Design for a 1.12-MW High-Speed PM Machine” , *IEEE Transactions on Industry Applications*, vol. 51, no. 5, pp. 3675-3685, 2015.

[8] Nannan Zhao, Z. Q. Zhu, and Weiguo Liu. “Rotor Eddy Current Loss Calculation and Thermal Analysis of Permanent Magnet Motor and Generator”, *IEEE Transactions on Magnetics*, vol. 47, no. 10, pp. 4199-4202, 2011.

[9] Ziyuan Huang, Bangcheng Han. “Effective approach for calculating critical speeds of high-speed permanent magnet motor rotor-shaft assemblies”, *IET Electr. Power Appl*., vol. 9, Iss. 9, pp. 628–633, 2015.

[10] Betotti G, pasquale M, PhysicalL “Interpretation of Induction and Frequency dependence of Power Losses in Soft Magnetic materials”. *IEEE Transactions on Magnetics*, vol. 28, no. 52, pp. 2787-2789, 1992.

[11] Do-K wan Hong, Jae-Hak Choi, Dong-Jun Kim, Yon-Do Chun, Byung-Chul Woo and Dae-Hyun Koo. “Development of high speed induction motor for spindle systems”, *IEEE Transaction. Magnetics*, vol. 49, no. 7, pp. 4088-4091, 2013.

[12] Wen Y. F. and Sun J. “Theoretical prediction of mechanical stability of ferromagnetic fcc Fe-Cu alloys form fist principles”, *Journal of Applies Physics*, vol. 111, no. 5, pp. 053517-053521, 2012.

[13] Kagimoto H, Miyagi D, Takahashi N, et al. "Effect of Temperature Dependence of Magnetic Properties on Heating Characteristics of Inductions Heater". *IEEE TRANSACTIONS ON MAGNETICS*. Vol. 46, no. 8, pp. 3018-3021, 2010.

[14] C. J Wu, S. Y. Lin, S. C. Chou, et al. "Temperature effects on the magnetic properties of silicon-steel sheets using standardized toroidal frame". *The Scientific World Journal*. 2014.

[15] Liyi Li, Guangjun Tan, Jiaxi Liu and Baoquan Kou, "An Optimal Pulse Width Modulation Method for High-speed Permanent Magnet Synchronous Motor", in *Third International Conference on Information Science and Technology March 23-25*, Yangzhou, Jiangsu, China, pp237-244, 2013;

[16] Jianning Dong, Yunkai Huang, Long Jin, Heyun Lin, and Hui Yang, Thermal Optimization of a High-Speed Permanent Magnet Motor, *IEEE Transactions on Magnetics*, vol. 50, no. 2, 2014, Article #: 7018504.

[17] Glynn J. Atkinson, Barrie C. Mecrow, Alan G. Jack, etc., The Analysis of Losses in High-Power Fault-Tolerant Machines for Aerospace Applications", *IEEE Transactions on Industry Applications*, vol. 42, no. 5, pp. 1162-1170, 2006.

[18] Fang Jiancheng, Liu Xiquan, Bangcheng Han, and Kun Wang, "Analysis of Circulating Current Loss for High-Speed Permanent Magnet Motor", IEEE Transactions on Magnetics, vol. 51, no. 1, January 2015.

[19] Jang S, ChoH, Choi S. "Design and analysis of a high-speed brushless DC motor for centrifugal compressor". IEEE Transactions on Magnetics, vol. 43, no. 6, pp. 2573-2575, 2007.

[20] D. Smith, B. Mecrow, G. Atkinson, A. Jack, and A. Mehna, "Shear stress concentrations in permanent magnet rotor sleeves," in *Proceeding XIX International Conference on Electrical Machines*, 2010, pp. 1–6.

[21] S. Jumayev, M. Merdzan, K. O. Boynov, J. J. H. Paulides, J. Pyrhönen, and E. A. Lomonova, The Effect of PWM on Rotor Eddy-Current Losses in High-Speed Permanent Magnet Machines, *IEEE Transactions on Magnetics*, vol. 51, no. 11, November 2015.

[22] Athanasios G. Sarigiannidis and Antonios G. Kladas, "Switching Frequency Impact on Permanent Magnet Motors Drive System for Electric Actuation Applications", *IEEE Transactions on Magnetics*, vol. 51, no. 3, march 2015, article #: 8202204.

[23] M. Etemadrezaei, J. J. Wolmarans, H. Polinder, and J. A. Ferreira, "Precise Calculation and Optimization of Rotor Eddy Current Losses in High Speed Permanent Magnet Machine", in *Electrical Machines (ICEM), 2012 XXth International Conference*, 2012, pp.1399-1404.

[24] Kondrath N, Kazimierczuk. M K. "Inductor winding loss owing to skin and proximity effects including harmonics in non-isolated pulse-width modulated dc-dc converters operating in continuous conduction mode". *Let Power Electronics*. vol. 3, no. 6, pp. 989-1000, 2010.

[25] Katsumi Yamazaki, and Atsushi Abe, Loss Investigation of Interior Permanent-Magnet Motors Considering Carrier Harmonics and Magnet Eddy Currents, *IEEE Transactions on Industry Applications*, vol. 45, no. 2, pp.659-665, 2009.

[26] Eri Maruyama, Satoshi Sumita and Akihito Nakahara, "Evaluation of Increasing Rates in Eddy-Current Loss of the Motor due to Carrier Frequency", in *Electrical Machines (ICEM), 2014 International Conference* , 2014, pp.1153-1157,

[27] ML. Sough , D. Depernet, F. Dubas, B. Boualem1, C. Espane, "Analytical Model of PMSM Designed for High-Frequency Operation Machine and Inverter sizing compromise", Energy Conversion Congress and Exposition (ECCE), 2011 IEEE, pp.1436-1440.

[28] S. M. Sharkh, A. Ali Qazalbash, N. T. Irenji, R. G. Wills , "Effect of Slot Configuration and Airgap and Magnet Thicknesses on Rotor Electromagnetic Loss in Surface PM Synchronous Machines", in *Electrical Machines and Systems (ICEMS), 2011 International Conference on*，2011, pp.1-6.

[29] Sisuda Chaithongsuk, Noureddine Takorabet, and Sangkla Kreuawan, Reduction of Eddy-Current Losses in Fractional-Slot Concentrated-Winding Synchronous PM Motors, *IEEE Transactions on Magnetics*, vol. 51, no. 3, March 2015, Article #: 8102204.

Yanan Yu received the B.S.,M.S. degree in electrical engineering and automation from Hunan University, Changsha, Hunan, China, in 2004 and 2010. Respectively. He is currently working toward the Ph.D. degree at Xi'an Jiaotong University, Xi'an, Shaanxi, China.

His research interests include optimal design of electrical machines.

Deliang Liang (M'11–SM'14) received the B.S., M.S., and Ph.D. degrees in electrical engineering from Xi'an Jiaotong University, Xi'an, China, in 1989, 1992, and 1996, respectively.

From 2001 to 2002, he was a Visiting Scholar with the Science Solution International Laboratory, Tokyo, Japan. Since 1999, he has been with the Department of Electrical Engineering, Xi'an Jiaotong University, where he is currently a Professor. His current research interests include optimal design, control, and simulation of electrical machines, and electrical machine technology in renewable energy.

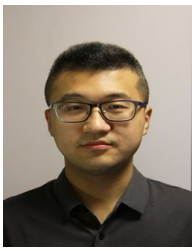

Zhe Liang received the B.S. degree in electrical engineering and automation from Xi'an Jiaotong University, Xi'an, Shaanxi, China, in 2012. He is currently working toward the Ph.D. degree at Xi'an Jiaotong University, Xi'an, Shaanxi, China.

His research interests include control of dual-channel PMSM, and fault-tolerant control strategy.

Qiji Ze received the B.S. degree in electrical engineering and automation from Xi'an Jiaotong University, Xi'an, Shaanxi, China, in 2011. He is currently working toward the Ph.D. degree at Xi'an Jiaotong University, Xi'an, Shaanxi, China.

His research interests include motion control, fault-tolerant control, doubly salient permanent magnet generator, and power electronics.